

pubs.acs.org/NanoLett Letter

Theory of Moiré Magnetism and Multidomain Spin Textures in Twisted Mott Insulator—Semimetal Heterobilayers

Mehmet Akif Keskiner,* Pouyan Ghaemi,* Mehmet Özgür Oktel,* and Onur Erten*



Cite This: Nano Lett. 2024, 24, 8575-8579



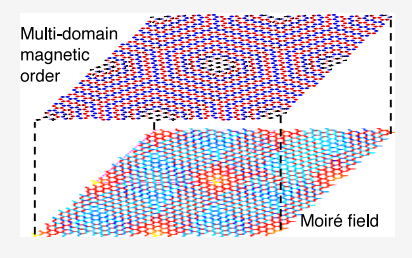
ACCESS I

Metrics & More

Article Recommendations

Supporting Information

ABSTRACT: Motivated by the recent experimental developments in van der Waals heterostructures, we investigate the emergent magnetism in Mott insulator—semimetal moiré superlattices by deriving effective spin models and exploring their phase diagram by Monte Carlo simulations. Our analysis indicates that the stacking-dependent interlayer Kondo interaction can give rise to different types of magnetic order, forming domains within the moiré unit cell. In particular, we find that the AB (AA) stacking regions tend to order (anti)ferromagnetically for an extended range of parameters. The remaining parts of the moiré unit cell form ferromagnetic chains that are coupled antiferromagnetically. We show that the decay length of the Kondo interaction can control the extent of these phases. Our



results highlight the importance of stacking-dependent interlayer exchange and the rich magnetic spin textures that can be obtained in van der Waals heterostructures.

KEYWORDS: moiré superlattices, 2D magnets, multidomain magnetic order, Kondo model

ondo model is a quintessential strongly correlated model that describes the interaction between localized magnetic moments and weakly interacting conduction electrons via an antiferromagnetic spin—spin interaction. Commonly utilized for lanthanide and actinide intermetallic compounds, the Kondo model can possess diverse phenomena such as heavy fermion formation, magnetic order, and unconventional superconductivity. Unlike other interacting models, such as the Hubbard model, the Kondo model exhibits a clear separation between the localized and the itinerant degrees of freedom, which allows for controlled calculations in certain limits. In the simplest form, the Kondo model involves only local interactions since both the localized moments and the conduction electrons originate from the f and d orbitals of the same lanthanite/actinide ions in most intermetallics.

Recently, an alternative route to realize the Kondo model has emerged in van der Waals (vdW) heterostructures. These synthetic Kondo lattices consist of a two-dimensional (2D) Mott insulator layer and a metallic or semimetallic layer as depicted in Figure 1(a,b). This route separates the Kondo model's two necessary degrees of freedom into different layers, in contrast to the intermetallics. For instance, a synthetic Kondo lattice has been realized in 1T-TaS₂/2H-TaS₂ bilayers where 1T-TaS₂ is a Mott insulator, and 2H-TaS₂ is a metal.⁴ STM experiments show a Kondo resonance in the tunneling spectrum appearing at around 27K.⁴ Similar behavior have also been observed in 1T/1H-TaSe₂⁵ and 1T/1H-TaS₂⁶ heterobilayers. Synthetic Kondo lattices may also be constructed in 2D magnetmetal/semimetal bilayers. As an example, a Kondo model with Kitaev intralayer interactions has been proposed for graphene/ α-RuCl₃ bilayers.⁷ Recent experimental and theoretical studies show that the interaction between graphene and α -RuCl₃ can

have a significant impact on the electronic and magnetic properties of both layers. $^{8-15}$

Compared to intermetallics, 2D vdW materials offer a broader tunability through gating, electric field, pressure, and strain. Their properties can be further controlled in moiré superlattices. Moiré superlattices can be formed by twisting or a lattice mismatch between the layers. For instance, the in-plane lattice constant of 1T-TaS₂ and 2H-TaS₂ are 3.36 and 3.316 Å respectively, which results in a moiré pattern with a periodicity of $L \sim 75$ unit cells. Even though the local stacking pattern depends on the origin of the moiré pattern, both mechanisms lead to similar features.

Motivated by these recent developments, we develop a model to study the magnetic order in synthetic Kondo moiré superlattices. We consider honeycomb lattices for both layers which are common among vdW magnets such as α -RuCl₃. We utilize an extended Kondo interaction since the local stacking order changes within the moiré unit cell. In the limit of small twist angles, only a few sites are aligned perfectly on top of each other, corresponding to AA and AB stacking regions. Our model incorporates both the Kondo interaction and the moiré potential. Our goal is not to simulate a material directly but it is to explore the magnetic phenomena that emerges at the intersection of these two mechanisms. For small twist angles, we

Received: April 2, 2024 Revised: July 2, 2024 Accepted: July 2, 2024 Published: July 8, 2024





Nano Letters pubs.acs.org/NanoLett Letter

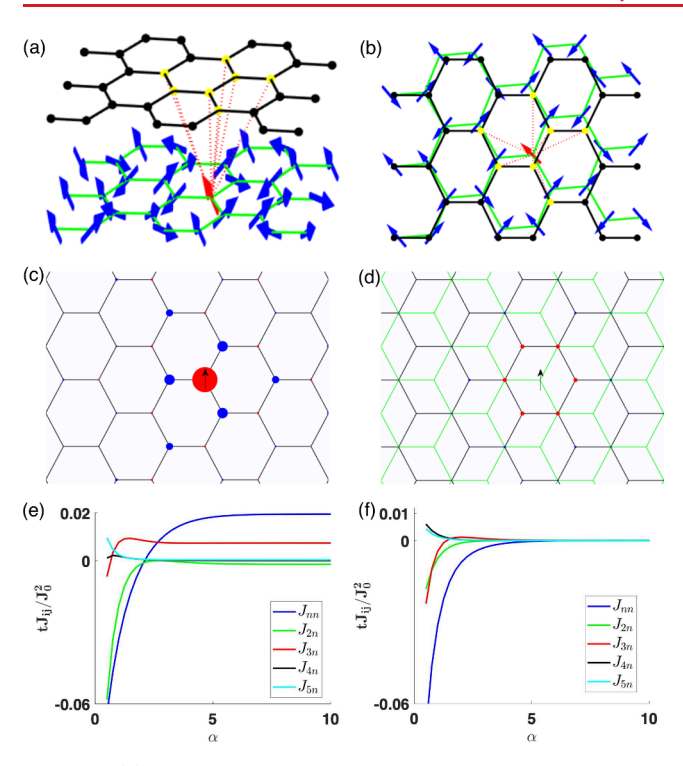


Figure 1. (a) Schematic representation of our model with conduction electrons on the upper layer and localized magnetic impurities on the lower layer, twisted relative to the upper layer. The blue arrows denote the local moments. The magnetic impurity, indicated by the red arrow, interacts only with the conduction electrons at the sites shown in yellow in the conduction layer. (b) Top view of our schematic. (c and d) Induced spin polarization for AA and AB stacking respectively for the inverse decay length $\alpha=3$. The impurity spin is marked with black arrow, and the area of the circles on each site is proportional to the spin polarization, where excess spin- \uparrow (spin- \downarrow) density is blue (red). (e and f) The RKKY coupling, J as a function of α for AA and AB stacking up to fifth nearest neighbor.

calculate the Ruderman-Kittel-Kasuya-Yosida (RKKY) interaction $^{20-22}$ via exact diagonalization up to third nearest neighbor and perform Monte Carlo simulations on the effective spin model to obtain the ground state spin texture. Our main results are as follows: (i) we show that the sign and the magnitude of the RKKY interaction varies depending on the local stacking order. (ii) Our Monte Carlo simulations indicate that the AA stacking regions order antiferromagnetically (AFM), whereas the AB regions order ferromagnetically (FM). The remaining parts of the moiré unit cell form ferromagnetic chains that are coupled antiferromagnetically (FMC). (iii) The extent of these regions varies with the inverse decay length of the Kondo interaction, α . For small α , FMC dominates the majority of the moiré unit cell, whereas for large α , FM, AFM, and FMC domains coexist.

We start by introducing the extended Kondo lattice Hamiltonian, which describes the interactions between localized magnetic moments with the conduction electrons in the moiré unit cell.

$$H = -t \sum_{\langle ij \rangle \sigma} (c_{ai\sigma}^{\dagger} c_{bj\sigma} + \text{H.c.}) - \mu \sum_{is\sigma} c_{is\sigma}^{\dagger} c_{is\sigma}$$
$$+ \sum_{ij;\alpha\beta} J_K(r_{ij}) c_{i\alpha}^{\dagger} \boldsymbol{\sigma}^{\alpha\beta} c_{i\beta} \cdot \mathbf{S}_j$$
(1)

where $c_{si\sigma}^{\dagger}$ is the creation operator for conduction electrons in $s = \{a, b\}$ sublattice and **S** is the spin operator of the local moments. r_{ij} represents the distance between two sites, $r_{ij} = |\mathbf{r}_i - \mathbf{r}_j|$. We consider the an extended Kondo coupling given by,

$$J_K(r_{ij}) = J_0 e^{-\alpha r_{ij}/a_0} \text{ for } r_{ij} \le \sqrt{3} a_0$$

$$= 0 \quad \text{otherwise}$$
(2)

where a_0 is the bond length on the honeycomb lattice and α is the inverse decay length. α is dimensionless since an explicit $1/a_0$ is included in the expression. α is proportional to the inverse length of interlayer hopping and may be controlled via pressure in vdW materials. The cutoff in the exchange coupling for $r_{ij} > \sqrt{3} \, a_0$ is imposed for practical computational purposes and we checked that our conclusions are independent of the cutoff. For the rest of the manuscript, we consider $\mu=0$, a semimetallic filling for the conduction electrons and use $J_0/t=10^{-2}$ to stay in the perturbative regime. Extended Kondo interaction is essential for the topological phases in heavy fermions. $^{24-27}$ It has also been investigated for nematic and higher angular momentum Kondo liquids.

RKKY interaction arises due to magnetic impurities interacting with conduction electrons which create net spin polarization. While the polarization propagates, it decays and undergoes Friedel oscillations. In Figure 1(c), we present the spin polarization when the magnetic impurity is perfectly aligned on top of a conduction site (AA stacking). The polarization is antiferromagnetic to the magnetic impurity due to the nature of the Kondo exchange coupling. The coupling flips sign at its nearest neighbors (NN) due to the large Dirac momentum (short wavelength) Friedel oscillations, similar to the effect of magnetic impurities in graphene. ³¹ In Figure 1(d), the magnetic impurity is placed at the center of the honeycomb (AB stacking). Note that the polarization is much smaller in this case since the local moment can only interact with conduction electrons at a distance $r = a_0$ and $J_K(r = a_0) \ll J_K(r = 0)$. The interaction of a second impurity with the spin-polarization induced by the first impurity leads to an effective interaction between the two local moments, which is known as RKKY interaction. In the absence of spin-orbit coupling, the RKKY interaction has SU(2) symmetry and can be expressed as a Heisenberg interaction, $J_{ii}S_{i}$ · S_i. We estimate the RKKY coupling constant via exact diagonalization following the procedure described in ref 31. We place two local moments at sites i and j and calculate the energy, including the interactions with the conduction electrons by aligning local moments parallel (E_{FM}) or antiparallel (E_{AFM}) . The RKKY coupling is given by the energy difference, $J_{ij} = (E_{EM})$ $-E_{AFM}$)/2 S^2 . In the following, we consider unit spins, S=1.

There are two key factors in determining the sign and the magnitude of the RKKY interaction, and both depend on the local stacking pattern. The magnitude of the RKKY interaction is primarily determined by the magnitude of r_{ij} . Since $J_K(r_{ij})$ decays exponentially with r_{ij} (eq 2), the RKKY interaction which is proportional to $[J_K(r_{ij})]^2$ is overall larger in AA stacking regions where $r_{ij}/a_0 \ll 1$ compared to AB stacking where $r_{ij}/a_0 \sim 1$ for one of the magnetic impurity. The sign of the interaction depends on whether the local moments primarily couple to the same or different conduction sites. Coupling to the same conduction site results in an FM RKKY interaction. Yet, if they couple to NN sites, the sign of the conduction electron polarization flips between the NN sites due to Friedel oscillations as discussed above and the RKKY interaction is AFM in this case. To illustrate these effects, we present the

Nano Letters pubs.acs.org/NanoLett Lette

RKKY interaction as a function of α for AA stacking and AB stacking for the "untwisted" system in Figure 1(e) and (f). For $\alpha \gg 1$, we recover the limit of local Kondo interaction where the exchange is only significant for $r_{ij}/a_0 \ll 1$. In particular, the AA stacking shows AFM NN and FM next nearest neighbor (NNN) interactions. These results are in agreement with previous estimations for RKKY interaction in graphene. On the contrary, the exchange constants are significantly smaller for the AB stacking region since $J_K(r=a_0)$ diminishes for $\alpha \gg 1$. However, unlike AA stacking, the NN exchange is FM since the local moments couple to the same conduction site.

For small α , the behavior of the exchange couplings is more complex due to multiple channels of Kondo interaction interfering with each other. The particular, we find that the sign of the NN interaction changes to FM for AA stacking for $\alpha < 2$ and several other exchange couplings seem to diverge for $\alpha < 1$. In order to keep $J_K(r=\sqrt{3}\,a_0)/J_K(r=0)$ small and justify the cutoff at $r>\sqrt{3}\,a_0$, we only consider $\alpha \geq 3$ for the reminder of the paper. To the best of our knowledge, the decay length dependence of the interlayer Kondo interaction in vdW materials has not been studied extensively. Still, we anticipate that $3 \leq \alpha \leq 10$ provides a regime that covers a large parameter space.

For small twist angles, the local stacking within a moiré unit cell can be described by a translational shift, $\mathbf{r}(R) \simeq \theta \, \hat{z} \times \mathbf{R}$ where \mathbf{R} and \mathbf{r} are the position within the moiré unit cell and translational shift, respectively. Therefore, a moiré unit cell with a large periodicity can be considered as a superposition of all possible stacking orders. We label the different regions in the moiré unit cell by the primary stacking orders, AA, AB, BA, and saddle point stacking (SP) in Figure 2(a). These regions

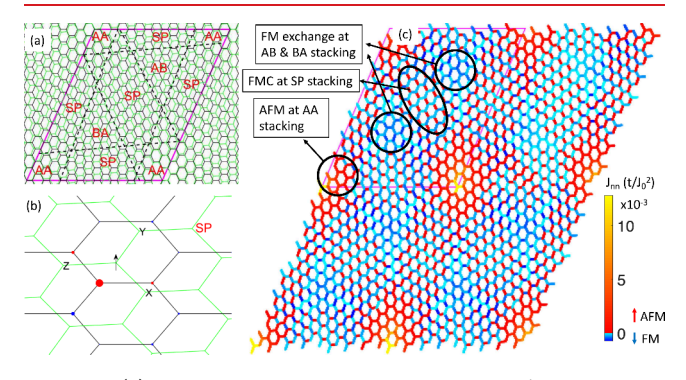


Figure 2. (a) Different stacking regions within a moiré unit cell: AA, AB, BA and saddle point (SP). (b) Conduction electron polarization induced by local moment for SP region for $\alpha = 4.6$. (c) NN RKKY interaction within a 2 × 2 moiré unit cell. Note that the dominant interaction is FM (AFM) for AB and BA (AA) regions. The SP regions 2 of the 3 bonds are FM, and the remaining bond is AFM which results in FM chains that are coupled antiferromagnetically.

exhibit different types of RKKY interactions. A local moment placed in AA or AB stacking regions polarizes the conduction electrons similar to the untwisted case as depicted in Figure 1(c) and (d). As a result, the effective magnetic interactions in these regions are similar to the untwisted case but superimposed in real space. The polarization induced by a local moment in the saddle point (SP) region is shown in Figure 2(b). It is noteworthy to emphasize that among the three NN sites, two of them couple primarily to the same conduction site and therefore exhibit FM exchange. However, for the other bonds, the local moments couple to the different conduction sites, which results

in AFM NN coupling. This leads to FM chains (FMC) in the SP region, as discussed below. We summarize these results in Figure 2(c), where we present the NN exchanges for all the bonds within a 2 \times 2 moiré unit cell for α = 4.6. We consider a twist angle θ = 4° with N = 394 unit cells for the remainder of the article, but our results are independent of the twist angle for small θ .

In order to determine the magnetic ground state of the moiré Kondo lattice, we derive the RKKY exchange couplings up to the third NN and perform classical Monte Carlo studies via the Metropolis algorithm. We include a small single site anisotropy term, $-J_A(S_i^z)^2$, which can naturally arise in real materials due to spin—orbit coupling, 36 to break the SU(2) symmetry of the model. We pick J_A much less than the smallest exchange coupling. Starting with random initial conditions, we perform 120,000 Monte Carlo updates at each temperature. We determine the ground state at $T/J_{\rm max}=10^{-4}$ where $J_{\rm max}$ is the maximum exchange coupling. Figure 3 depicts the Monte Carlo

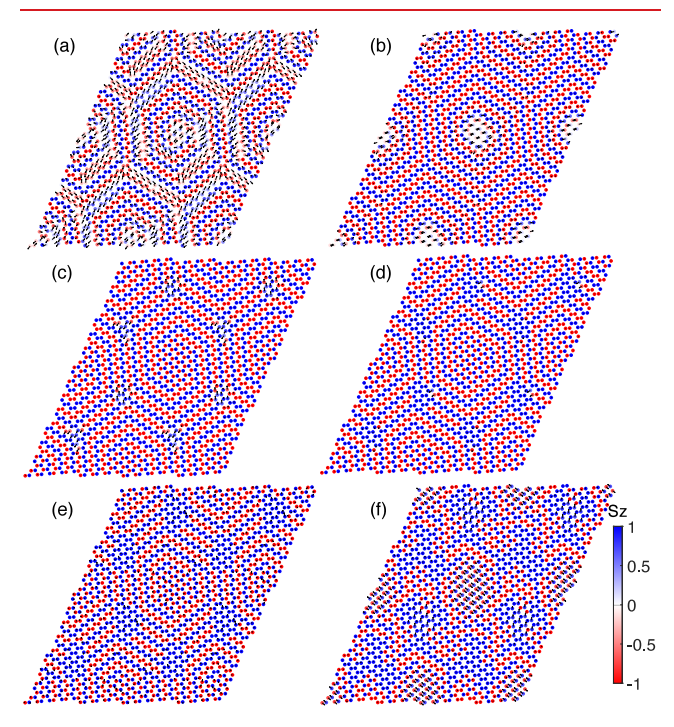


Figure 3. Monte Carlo snapshots for the ground state spin textures for $\alpha=3$, 3.2, 4.3, 4.6, 5, 10 for (a-f), respectively. For $\alpha<4$, the ground state primarily consists of ferromagnetic chains that are coupled antiferromagnetically with a small AFM region at the AA stacking. For $\alpha>4$, FM (AFM) regions grow at AB and BA (AA) stacking regions within the moiré unit cell. The color plot shows the z-component of the magnetization, whereas the arrows show the in-plane component.

snapshots of the ground state spin configurations for different values of α . We demonstrate that for $\alpha < 4$, the ground state primarily consists of FMC throughout the moiré unit cell and a small fraction of AFM around the AA stacking regions. For $\alpha > 4$, the FMC starts to shrink and FM (AFM) regions grow around AB and BA (AA) regions. FMC regions almost fully disappear as depicted in Figure 3(f) for $\alpha = 10$. Note that for such values of α , RKKY coupling essentially vanishes except for the AA stacking regions.

In order to quantify these trends, we calculate the magnetization, $\langle M^{\alpha} \rangle = \left\langle \frac{1}{N} \sum_{i} S_{i}^{\alpha} \right\rangle$, and the static spin structure factor $S(\mathbf{q}) = (1/N^{2}) \langle \sum_{\beta=x,y,x} | \sum_{i} S_{i}^{\beta} e^{-i\mathbf{q}\cdot\mathbf{r}_{i}}|^{2} \rangle$ of the ground state. $S(\mathbf{q})$

Nano Letters pubs.acs.org/NanoLett Letter

exhibits peaks at $\mathbf{q} = (0,0)$, $\{\pm \mathbf{b}_{1(2)}/2, \pm (\mathbf{b}_1 + \mathbf{b}_2)/2\}$, $\{\pm \mathbf{b}_{1(2)}, \pm (\mathbf{b}_1 + \mathbf{b}_2)\}$, where $\mathbf{b}_{1/2}$ are the reciprocal lattice vectors, corresponding to FM, FMC and AFM orders respectively (see Supporting Information for details). We present the amplitude of these peaks in Figure 4(a). The $\mathbf{q} = (0,0)$ component of $S(\mathbf{q})$

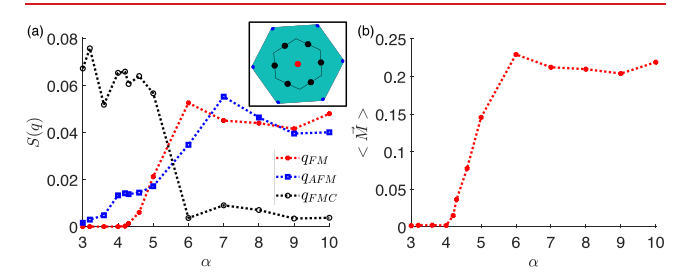


Figure 4. (a) Static spin structure factor $S(\mathbf{q})$ as a function of α , for $\mathbf{q} = (0,0)$ (red), $\mathbf{q} = \pm \mathbf{b}_1, \pm \mathbf{b}_2, \pm (\mathbf{b}_1 + \mathbf{b}_2)$ (blue) and $\mathbf{q} = \pm \mathbf{b}_1/2, \pm \mathbf{b}_2/2, \pm (\mathbf{b}_1 + \mathbf{b}_2)/2$ (black) corresponding to FM, AFM and FMC order, respectively. The inset shows the position of these wave vectors in the extended Brillouin zone. (b) Net magnetization as a function of α . Note that the $\mathbf{q} = (0,0)$ component of the spin structure factor is the square of magnetization.

is the square of the magnetization as shown in Figure 4(b). The spin structure factor also shows that the FMC is the primary order for α < 6. For α > 6, FMC regions shrink and AFM, FM regions grow rapidly. As shown in Figure 4(b), the magnetization grows for α > 4 and saturates at about M/S = 0.2-0.25.

Experimental detection of complex magnetic textures in the 2D limit is challenging. Although a variety of noncoplanar magnetic structures have been predicted in moiré superlattices of vdW magnets, 33,34,37-47 only few of these phases have been observed experimentally by magnetic circular dichroism, 48 magneto-optical Kerr effect 49 and diamond NV magnetometry. 50 Our simulations indicate that FM and AFM domains can form within a single moiré unit cell. We expect that these techniques should be able to detect the FM domains. For instance, diamond NV magnetometry can have resolution down to 20-50 nm, which may be compatible with the domain sizes for large moiré periodicity.⁵⁰ Even though our model and simulations does not apply to a material system directly, we anticipate similar multidomain magnetic order may be realized in synthetic moiré Kondo lattices. The fact that moiré patterning can induce magnetic order is unexpected and the complex magnetic structures are novel and can lead to the foundations for other spin textures such as skyrmions in moiré Kondo lattices. 34,36

In conclusion, we presented a theoretical framework for magnetic order in synthetic moiré Kondo lattices consisting of Mott insulator and semimetal vdW layers. We showed that the stacking-dependent Kondo interaction can give rise to various types of magnetic order. In particular, we demonstrated that the decay length of the Kondo interaction can control the magnetic textures. Interesting future directions include realistic simulations of material platforms, investigating the effects of pressure and gating, and the competition between heavy fermion formation and magnetism in these systems.

ASSOCIATED CONTENT

Supporting Information

The Supporting Information is available free of charge at https://pubs.acs.org/doi/10.1021/acs.nanolett.4c01574.

Details of the static spin structure factor calculation (PDF)

AUTHOR INFORMATION

Corresponding Authors

Mehmet Akif Keskiner — Department of Physics, Bilkent University, Ankara 06800, Türkiye; Email: akif.keskiner@ bilkent.edu.tr

Pouyan Ghaemi — Physics Department, City College of the City University of New York, New York, New York 10031, United States; Physics Program, Graduate Center of City University of New York, New York, New York 10031, United States; Email: pghaemi@ccny.cuny.edu

Mehmet Özgür Oktel — Department of Physics, Bilkent University, Ankara 06800, Türkiye; ⊚ orcid.org/0000-0001-8921-8388; Email: oktel@fen.bilkent.edu.tr

Onur Erten — Department of Physics, Arizona State University, Tempe, Arizona 85287, United States; oorcid.org/0000-0002-1944-239X; Email: onur.erten@asu.edu

Complete contact information is available at: https://pubs.acs.org/10.1021/acs.nanolett.4c01574

Author Contributions

M. A. Keskiner performed the exact diagonalization and Monte Carlo simulations. M. Ö. Oktel, Pouyan Ghaemi, and Onur Erten conceptualized the research. All authors analyzed the results and contributed to writing the manuscript.

Notes

The authors declare no competing financial interest.

ACKNOWLEDGMENTS

We thank Cemal Yalabik and Erik Henriksen for fruitful discussions. O.E. acknowledges support from National Science Foundation Award No. DMR-2234352. M.A.K. and M.O.O. are partially supported by TUBITAK 1001 Grant No 122F346. P.G. acknowledges support from NSF DMR-2130544 and infrastructural support from NSF HRD-2112550 (NSF CREST Center IDEALS).

REFERENCES

- (1) Stewart, G. R. Heavy-fermion systems. Rev. Mod. Phys. 1984, 56, 755-787.
- (2) Coleman, P. Introduction to Many-Body Physics; Cambridge University Press, 2015.
- (3) Wirth, S.; Steglich, F. Exploring heavy fermions from macroscopic to microscopic length scales. *Nature Reviews Materials* **2016**, *1*, 16051.
- (4) Ayani, C. G.; Pisarra, M.; Ibarburu, I. M.; Garnica, M.; Miranda, R.; Calleja, F.; Martin, F.; Vazquez de Parga, A. L. Probing the Phase Transition to a Coherent 2D Kondo Lattice. *Small* **2023**, 2303275.
- (5) Wan, W.; Harsh, R.; Meninno, A.; Dreher, P.; Sajan, S.; Guo, H.; Errea, I.; de Juan, F.; Ugeda, M. M. Evidence for ground state coherence in a two-dimensional Kondo lattice. *Nat. Commun.* **2023**, *14*, 7005.
- (6) Vaňo, V.; Amini, M.; Ganguli, S. C.; Chen, G.; Lado, J. L.; Kezilebieke, S.; Liljeroth, P. Artificial heavy fermions in a van der Waals heterostructure. *Nature* **2021**, *599*, 582–586.
- (7) Jin, H.-K.; Knolle, J. Flat and correlated plasmon bands in graphene/ α -RuCl₃ heterostructures. *Phys. Rev. B* **2021**, *104*, No. 045140.
- (8) Mashhadi, S.; Kim, Y.; Kim, J.; Weber, D.; Taniguchi, T.; Watanabe, K.; Park, N.; Lotsch, B.; Smet, J. H.; Burghard, M.; et al. others Spin-split band hybridization in graphene proximitized with α -RuCl3 nanosheets. *Nano Lett.* **2019**, *19*, 4659–4665.
- (9) Zhou, B.; Balgley, J.; Lampen-Kelley, P.; Yan, J.-Q.; Mandrus, D. G.; Henriksen, E. A. Evidence for charge transfer and proximate

Nano Letters pubs.acs.org/NanoLett Letter

- magnetism in graphene— α RuCl 3 heterostructures. *Phys. Rev. B* **2019**, 100, 165426.
- (10) Biswas, S.; Li, Y.; Winter, S. M.; Knolle, J.; Valentí, R. Electronic Properties of α RuCl 3 in proximity to graphene. *Phys. Rev. Lett.* **2019**, 123, 237201.
- (11) Rizzo, D. J.; et al. Charge-Transfer Plasmon Polaritons at Graphene/ α -RuCl3 Interfaces. *Nano Lett.* **2020**, *20*, 8438–8445.
- (12) Gerber, E.; Yao, Y.; Arias, T. A.; Kim, E.-A. Ab Initio Mismatched Interface Theory of Graphene on α RuCl 3: Doping and Magnetism. *Phys. Rev. Lett.* **2020**, *124*, 106804.
- (13) Leeb, V.; Polyudov, K.; Mashhadi, S.; Biswas, S.; Valentí, R.; Burghard, M.; Knolle, J. Anomalous quantum oscillations in a heterostructure of graphene on a proximate quantum spin liquid. *Phys. Rev. Lett.* **2021**, *126*, No. 097201.
- (14) Balgley, J.; Butler, J.; Biswas, S.; Ge, Z.; Lagasse, S.; Taniguchi, T.; Watanabe, K.; Cothrine, M.; Mandrus, D. G.; Velasco, J., Jr others Ultrasharp Lateral p—n Junctions in Modulation-Doped Graphene. *Nano Lett.* **2022**, 22, 4124—4130.
- (15) Shi, J.; MacDonald, A. Magnetic states of graphene proximitized Kitaev materials. *Phys. Rev. B* **2023**, *108*, No. 064401.
- (16) Liu, Y.; Weiss, N. O.; Duan, X.; Cheng, H.-C.; Huang, Y.; Duan, X. Van der Waals heterostructures and devices. *Nature Reviews Materials* **2016**, *1*, 16042.
- (17) He, F.; Zhou, Y.; Ye, Z.; Cho, S.-H.; Jeong, J.; Meng, X.; Wang, Y. Moiré Patterns in 2D Materials: A Review. *ACS Nano* **2021**, *15*, 5944–5058
- (18) Mattheiss, L. F. Band Structures of Transition-Metal-Dichalcogenide Layer Compounds. *Phys. Rev. B* **1973**, *8*, 3719–3740.
- (19) Clerc, F.; Bovet, M.; Berger, H.; Despont, L.; Koitzsch, C.; Gallus, O.; Patthey, L.; Shi, M.; Krempasky, J.; Garnier, M. G.; Aebi, P. Spin—orbit splitting in the valence bands of 1T-TaS2 and 1T-TaSe2. *J. Phys.: Condens. Matter* **2004**, *16*, 3271.
- (20) Ruderman, M. A.; Kittel, C. Indirect Exchange Coupling of Nuclear Magnetic Moments by Conduction Electrons. *Phys. Rev.* **1954**, 96, 99–102.
- (21) Yosida, K. Magnetic Properties of Cu-Mn Alloys. *Phys. Rev.* **1957**, 106, 893–898.
- (22) Kasuya, T. A Theory of Metallic Ferro- and Antiferromagnetism on Zener's Model. *Prog. Theor. Phys.* **1956**, *16*, 45–57.
- (23) Akram, M.; Kapeghian, J.; Das, J.; Valentí, R.; Botana, A. S.; Erten, O. Theory of Moiré Magnetism in Twisted Bilayer α -RuCl3. *Nano Lett.* **2024**, 24, 890–896.
- (24) Dzero, M.; Xia, J.; Galitski, V.; Coleman, P. Topological Kondo Insulators. *Annual Review of Condensed Matter Physics* **2016**, 7, 249–280
- (25) Alexandrov, V.; Coleman, P.; Erten, O. Kondo Breakdown in Topological Kondo Insulators. *Phys. Rev. Lett.* **2015**, *114*, 177202.
- (26) Ghazaryan, A.; Nica, E. M.; Erten, O.; Ghaemi, P. Shadow surface states in topological Kondo insulators. *New J. Phys.* **2021**, *23*, 123042.
- (27) Lai, H.-H.; Grefe, S. E.; Paschen, S.; Si, Q. Weyl-Kondo semimetal in heavy-fermion systems. *Proc. Natl. Acad. Sci. U. S. A.* **2018**, 115, 93–97.
- (28) Vijayvargia, A.; Erten, O. Nematic heavy fermions and coexisting magnetic order in CeSiI. *Phys. Rev. B* **2024**, *109*, No. L201118.
- (29) Ghaemi, P.; Senthil, T. Higher angular momentum Kondo liquids. *Phys. Rev. B* **2007**, *75*, 144412.
- (30) Ghaemi, P.; Senthil, T.; Coleman, P. Angle-dependent quasiparticle weights in correlated metals. *Phys. Rev. B* **2008**, *77*, 245108.
- (31) Black-Schaffer, A. M. RKKY coupling in graphene. *Phys. Rev. B* **2010**, *81*, 205416.
- (32) Ahamed, S.; Moessner, R.; Erten, O. Why rare-earth ferromagnets are so rare: Insights from the *p*-wave Kondo model. *Phys. Rev. B* **2018**, 98, No. 054420.
- (33) Akram, M.; LaBollita, H.; Dey, D.; Kapeghian, J.; Erten, O.; Botana, A. S. Moiré Skyrmions and Chiral Magnetic Phases in Twisted CrX3 (X = I, Br, and Cl) Bilayers. *Nano Lett.* **2021**, *21*, 6633–6639.
- (34) Akram, M.; Erten, O. Skyrmions in twisted van der Waals magnets. *Phys. Rev. B* **2021**, *103*, No. L140406.

- (35) McGilly, L. J.; et al. Visualization of moiré superlattices. *Nat. Nanotechnol.* **2020**, *15*, 580–584.
- (36) Banerjee, S.; Rowland, J.; Erten, O.; Randeria, M. Enhanced Stability of Skyrmions in Two-Dimensional Chiral Magnets with Rashba Spin-Orbit Coupling. *Phys. Rev. X* **2014**, *4*, No. 031045.
- (37) Tong, Q.; Liu, F.; Xiao, J.; Yao, W. Skyrmions in the moiré of van der Waals 2D Magnets. *Nano Lett.* **2018**, *18*, 7194–7199.
- (38) Hejazi, K.; Luo, Z.-X.; Balents, L. Noncollinear phases in moiré magnets. *Proc. Natl. Acad. Sci. U. S. A.* **2020**, *117*, 10721–10726.
- (39) Hejazi, K.; Luo, Z.-X.; Balents, L. Heterobilayer moiré magnets: Moiré skyrmions and commensurate-incommensurate transitions. *Phys. Rev. B* **2021**, *104*, L100406.
- (40) Xiao, F.; Chen, K.; Tong, Q. Magnetization textures in twisted bilayer CrX₃(X = Br, I). *Phys. Rev. Research* **2021**, 3, No. 013027.
- (41) Xiao, F.; Chen, K.; Tong, Q. Magnetization textures in twisted bilayer CrX₃(X = Br, I). *Phys. Rev. Res.* **2021**, *3*, No. 013027.
- (42) Ghader, D.; Jabakhanji, B.; Stroppa, A. Whirling interlayer fields as a source of stable topological order in moiré CrI3. *Communications Physics* **2022**, *5*, 192.
- (43) Zheng, F. Magnetic Skyrmion Lattices in a Novel 2D-Twisted Bilayer Magnet. *Adv. Funct. Mater.* **2023**, *33*, 2206923.
- (44) Kim, K.-M.; Kiem, D. H.; Bednik, G.; Han, M. J.; Park, M. J. Ab Initio Spin Hamiltonian and Topological Noncentrosymmetric Magnetism in Twisted Bilayer CrI3. *Nano Lett.* **2023**, 23, 6088–6094.
- (45) Fumega, A. O.; Lado, J. L. Moiré-driven multiferroic order in twisted CrCl3, CrBr3 and CrI3 bilayers. 2D Materials 2023, 10, No. 025026.
- (46) Nica, E.; Akram, M.; Vijayvargia, A.; Moessner, R.; Erten, O. Kitaev spin-orbital bilayers and their moiré superlattices. *npj Quantum Mater.* **2023**, *8*, 9.
- (47) Vijayvargia, A.; Nica, E. M.; Moessner, R.; Lu, Y.-M.; Erten, O. Magnetic fragmentation and fractionalized Goldstone modes in a bilayer quantum spin liquid. *Phys. Rev. Res.* **2023**, *5*, No. L022062.
- (48) Xu, Y.; Ray, A.; Shao, Y.-T.; Jiang, S.; Lee, K.; Weber, D.; Goldberger, J. E.; Watanabe, K.; Taniguchi, T.; Muller, D. A.; Mak, K. F.; Shan, J. Coexisting ferromagnetic—antiferromagnetic state in twisted bilayer CrI3. *Nat. Nanotechnol.* **2022**, *17*, 143–147.
- (49) Xie, H.; Luo, X.; Ye, Z.; Sun, Z.; Ye, G.; Sung, S. H.; Ge, H.; Yan, S.; Fu, Y.; Tian, S.; Lei, H.; Sun, K.; Hovden, R.; He, R.; Zhao, L. Evidence of non-collinear spin texture in magnetic moiré superlattinices. *Nat. Phys.* **2023**, *19*, 1150–1155.
- (50) Song, T.; Sun, Q.-C.; Anderson, E.; Wang, C.; Qian, J.; Taniguchi, T.; Watanabe, K.; McGuire, M. A.; Stöhr, R.; Xiao, D.; Cao, T.; Wrachtrup, J.; Xu, X. Direct visualization of magnetic domains and moiré; magnetism in twisted 2D magnets. *Science* **2021**, *374*, 1140–1144.